

First Row Transition Metals in Olefin Metathesis: The Role of Iron and Manganese

Artur Brotons Rufes,^[a] Juan Pablo Martínez,^[b] Nicolas Joly,^[a, c] Sylvain Gaillard,^[c] Jean Luc Renaud,^{*,[c, d]} Sergio Posada Pérez,^{*,[a, e]} and Albert Poater^{*,[a]}

Dedicated to Prof. Agustí Lledós for his 70th anniversary

Olefin metathesis has traditionally been dominated by molybdenum and ruthenium-based catalysts, but the pursuit of sustainable and earth-abundant alternatives has driven interest in first-row transition metals particularly iron. While iron is an attractive candidate due to its abundance, low toxicity, and cost-effectiveness, significant challenges hinder its successful implementation in metathesis reactions. This review examines the electronic and structural properties of iron that contribute to its catalytic limitations, including high-spin configurations, weak metal-alkylidene interactions, and a pronounced tendency toward cyclopropanation. Computational and experimental efforts to overcome these obstacles are discussed, focusing on ligand design strategies and mechanistic insights. Addition-

ally, the potential of manganese as an alternative to iron is explored. This work underscores the complexities of first-row transition metal catalysts in olefin metathesis and highlights future directions for achieving practical, efficient iron-based systems. Future research should focus on refining ligand architectures to stabilize key intermediates, leveraging computational insights to predict reactivity trends, and further investigating the role of metal oxidation states in metathesis activity. While the transition to first-row transition metals remains a challenge, ongoing advancements continue to push the boundaries of sustainable catalysis, bringing the dream of practical iron- or manganese-based olefin metathesis closer to reality.

1. Introduction

A core principle of green chemistry is the use of safe, removable reagents in synthetic processes. One of the most promising

strategies to achieve this is employing first-row transition metals as catalysts. Metals such as iron, manganese, and copper are not only more abundant but also less toxic and generally more environmentally friendly than their heavier counterparts.^[1,2] By leveraging their unique catalytic properties, chemists aim to develop more sustainable methodologies that reduce waste and minimize dependence on conventional synthetic approaches.

Replacing traditional metals like ruthenium,^[3–7] molybdenum,^[8–10] and tungsten^[11,12] with iron in organic and organometallic catalysis offers significant advantages,^[13–16] and in some cases, they are even competitive with second- and third-row homologues, such as the (de)hydrogenative Knölker catalysts^[17] and their derivatives,^[18,19] or in Wacker type oxidations;^[20,21] and if not more efficient, at least more selective in C–H bond oxidations.^[22] As the most abundant transition metal on earth, iron provides a cost-effective and sustainable alternative addressing both economic and environmental concerns associated with rare and precious metals. Additionally, iron's diverse oxidation states and coordination chemistry enable unique reactivity and selectivity patterns, paving the way for innovative catalytic applications. The development of efficient iron-based catalysts has the potential to revolutionize organometallic catalysis, making it more sustainable, widely accessible, and aligned with green chemistry principles.

First-row transition metals exhibit distinct chemical behavior compared to other d-block elements. Notably, their d-orbitals experience smaller splitting, allowing access to high-spin configurations. This leads to an increased number of stable non-singlet multiplicity species, expanding their reactivity. However, this characteristic can pose challenges when substituting larger

[a] A. B. Rufes, N. Joly, S. P. Pérez, A. Poater
Institut de Química Computacional i Catàlisi and Departament de Química,
Universitat de Girona, c/ M^a Aurèlia Capmany 69, Girona17003, Catalonia,
Spain
E-mail: sergio.posada.perez@vub.be
albert.poater@udg.edu

[b] J. P. Martínez
Centre of New Technologies, University of Warsaw, Banacha 2c,
Warszawa02–097, Poland

[c] N. Joly, S. Gaillard, J. L. Renaud
ENSICAEN, Univ Caen Normandie, Univ Rouen Normandie, INSA Rouen
Normandie, CNRS, Institut CARMen UMR 6064, 6 bd. du Maréchal Juin, Caen
14050, France
E-mail: jean-luc.renaud@sorbonne-universite.fr

[d] J. L. Renaud
Sorbonne Université, CNRS, Institut Parisien de Chimie Moléculaire, UMR
8232, Paris75005, France

[e] S. P. Pérez
Department of General Chemistry (ALGC), Vrije Universiteit Brussel (VUB),
Pleinlaan 2, Brussels1050, Belgium

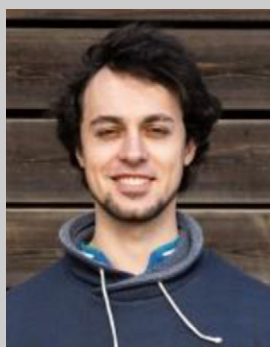
Supporting information for this article is available on the WWW under
<https://doi.org/10.1002/cctc.202500570>

© 2025 The Author(s). ChemCatChem published by Wiley-VCH GmbH. This is
an open access article under the terms of the [Creative Commons Attribution](#)
License, which permits use, distribution and reproduction in any medium,
provided the original work is properly cited.

elements within the same group, as unintended reactivity may arise.

A key distinction between traditional metal and iron complexes in olefin metathesis lies in the nature of the carbene bond in the alkylidene.^[23–25] This bond is crucial to the 14-electron intermediate, a fundamental component of Chauvin's olefin metathesis mechanism (Scheme 1),^[26] which consists

of a 14-electron intermediate that leads to the formation of the metallacycle through a coordination intermediate; upon opening of the four-membered ring, a second coordination intermediate is formed, ultimately yielding another 14-electron species. Organometallic carbene ligands are classified as Fischer or Schrock carbenes (see Figure 1)^[27] with Schrock carbenes being essential for active olefin metathesis catalysts. In



Dr. Artur Brotons-Rufes is a Spanish chemist specializing in computational and organometallic chemistry. He earned his Ph.D. from the University of Girona in 2024, under the supervision of Dr. Albert Poater and Dr. Sergio Posada-Pérez. His research focuses on density functional theory (DFT) simulations applied to catalysis and energy materials. He has co-authored publications on topics such as olefin metathesis, ionic liquids for gas capture, and lithium-ion battery cathodes. In 2023, he received a prize at the XXXIX Bienal de the Real Sociedad Española de Química. Currently, he is affiliated with Università degli Studi di Salerno with Dr. Chiara Costabile.



Dr. Juan Pablo Martínez earned a joint Ph.D. in Chemistry from the University of Girona (Catalonia, Spain, 2016) and Vrije Universiteit Amsterdam (The Netherlands, 2017). In 2021, he joined the Centre of New Technologies at the University of Warsaw (CeNT-UW) as a postdoctoral researcher, where he focused on catalyzed metathesis reactions. He later advanced to the position of Associate Professor. In 2025, he was appointed Principal Investigator at CeNT-UW for a project funded by the Polish National Science Centre, dedicated to the ethenolysis of renewable oils. His research centers on sustainable catalysis and the transformation of bio-based feedstocks.



Dr. Nicolas Joly earned his Master's degree in Molecular Chemistry in 2020 from the École Nationale Supérieure de Chimie de Rennes (ENSCR). He completed a joint PhD in Chemistry in 2023 between the University of Caen Normandy and the University of Girona, under the supervision of Prof. Jean-Luc Renaud and Dr. Albert Poater. He is currently a postdoctoral researcher, having worked with Dr. Thibault Cantat at CEA Paris-Saclay, and, since 2025,

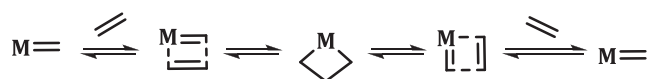


with Prof. Thomas Poisson and Prof. Philippe Jubault at the University of Rouen. His research focuses on synthetic methodologies and catalysis involving sustainable chemical transformations.

Dr. Sylvain Gaillard received his PhD from the Université Paul Cézanne/Aix-Marseille III in 2007. After a first postdoctoral position at the ENSCR in Rennes, he pursued with a second post-doctoral position at the University of St Andrews. In 2010, he accepted an associate professor position in the group of Pr Jean Luc Renaud at the University of Caen Normandy. He is currently conducting an independent carrier focusing on the molecular design of transition metal complexes for their photophysical properties applied in photocatalysis, hybrid materials and biological activities.



Prof. Jean-Luc Renaud received his PhD in 1998 under the guidance of Dr. Aubert and Prof. Malacria. Following a Lavoisier Postdoctoral Fellowship with Prof. Lautens at the University of Toronto in 1999, he joined Prof. Riant's group at the University of Louvain-La-Neuve. In 2000, he became Maître de Conférences at the University of Rennes and, in 2008, was appointed Full Professor at the University of Caen Normandy. Since October 2023, he has also been an invited researcher at the Institut Parisien de Chimie Moléculaire (IPCM), Sorbonne University. His research focuses on organometallic, organocatalytic, and photoredox catalysis applied to bioactive molecule synthesis.



Scheme 1. Chauvin mechanism in olefin metathesis.

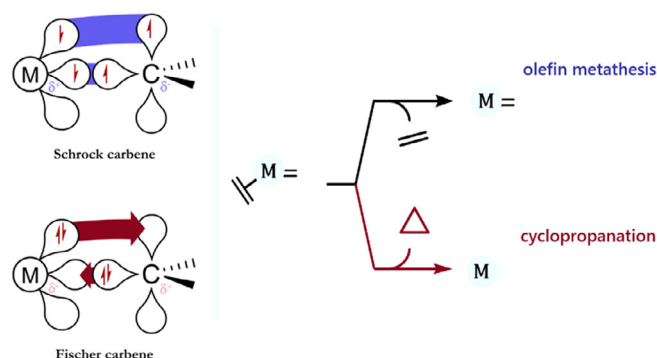


Figure 1. Fischer and Schrock carbene electronic structure representation.

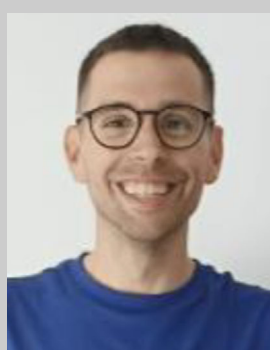
many olefin metathesis catalyst activation studies, ethyl vinyl ether (EVE) is commonly used to ensure that only a single reaction turnover occurs, corresponding to the preactivation step. This is because ylidenes groups with strong electron-withdrawing substituents generate Fischer carbenes in traditional ruthenium-based catalysts. The inactivity of these catalysts stems from the low electron density on the carbene carbon, which prevents the cycloreversion step in the olefin metathesis mechanism.

The metal to which the alkylidene is coordinated also influences the nature of the carbene.^[16] Due to weaker orbital overlap between the metal center and the carbon atom, many Schrock carbenes transition into Fischer carbenes when the metal is replaced with the smaller iron nucleus. As a result, the alkylidene bond in iron complexes is significantly weaker,

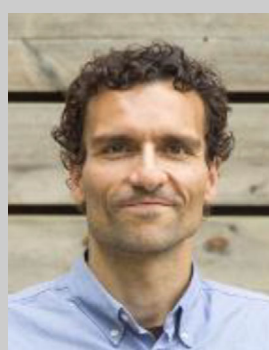
exhibiting a lower bond dissociation energy (BDE) than in other transition metals. Furthermore, transition metals such as iron are characterized by smaller ligand field splitting, which allows high-spin configurations and access to triplet states. These electronic properties render iron catalysts inactive in olefin metathesis processes while simultaneously promoting undesirable cyclopropanation reactions (Figure 1, right).^[28,29]

Research in this area has focused on mitigating the unfavorable effects associated with incorporating iron into olefin metathesis systems. This has been achieved through tailored ligand designs that impose specific constraints on the coordination environment. Computational chemistry has been instrumental in this effort, providing valuable insights into the behavior of iron-based catalysts. Recent partial successes in this field are largely attributed to theoretical analyses, which continue to guide experimental advancements. These findings highlight the critical role of theoretical frameworks in improving the efficiency and applicability of iron catalysts in olefin metathesis reactions. In addition, olefin metathesis supports green chemistry by being catalytic and streamlining synthesis, minimizing waste, and inorganic byproducts.^[30,31] Its precision and functional group tolerance make it a powerful tool for converting simple molecules into complex structures efficiently.^[32] However, before transitioning to first-row transition metals, it is important to acknowledge that olefin metathesis, despite the success of existing catalysts, still presents well-documented drawbacks, particularly related to decomposition, which remain unresolved,^[33–38] even after extensive experimental^[39,40] and computational insights.^[41,42]

The article will primarily review computational studies on iron in olefin metathesis catalysis aligned with the review published in 2022 by Meyer and coworkers^[43] followed by calculations to corroborate the main conclusions, and finally the current limits and next challenges with other first row transition metals will be delineated.



Dr. Sergio Posada-Pérez is a Spanish chemist specializing in theoretical and computational chemistry. He earned his PhD from the University of Barcelona in 2018 supervised by Prof. Francesc Illas, focusing on developing cost-effective catalysts for greenhouse gas conversion. He has held postdoctoral positions at Université Catholique de Louvain, Universitat de Girona, and currently at Vrije Universiteit Brussel under the EUTOPIA-SIF fellowship. His research encompasses heterogeneous catalysis, electrocatalysis, and energy storage materials, contributing to over 40 publications. Dr. Posada-Pérez's work aims to advance sustainable chemical processes and green energy solutions.



Dr. Albert Poater earned his PhD in Chemistry from the University of Girona in 2006. Following research stays in Chile, Montpellier, and a postdoctoral position at the University of Salerno, he joined the University of Girona as a Ramón y Cajal fellow in 2010. He has held visiting researcher positions in Saudi Arabia and Toulouse, and in 2019 was appointed Serra Húnter Associate Professor. That same year, he received the prestigious ICREA Acadèmia award. Author of over 350 publications with 16,000 citations (H-index: 68), his work centers on DFT-based studies in inorganic and organometallic catalysis, with a focus on green chemistry.

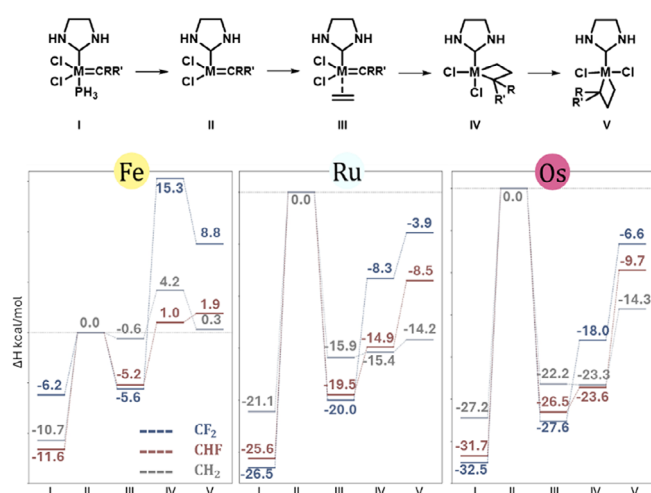


Figure 2. Thermodynamic profile for $\text{CRR}' = \text{CH}_2$ (grey), CHF (red), and CF_2 (blue) at the CCSD(T)/aug-cc-pVDZ(-PP)//B3LYP/aug-cc-pVDZ level of theory with enthalpies in kcal/mol by Dixon and coworkers.^[45]

2. Computational Insight in Iron Olefin Metathesis

Initial evaluations of iron catalysts primarily focused on assessing the thermodynamics of a Chauvin-like mechanism by substituting iron into well-established ruthenium-based systems. However, the inherently complex electronic behavior of iron poses challenges for traditional density functional theory (DFT) approaches, particularly in determining the ground-state multiplicity.

To address these limitations, Dixon and coworkers conducted a series of studies employing post-Hartree-Fock, wavefunction-based, highly accurate electron correlation methods, specifically coupled-cluster with single, double, and perturbative triple excitations (CCSD(T)). Their research focused on second-generation Grubbs-type catalysts, simplifying ligand structures to reduce the computational cost of these high-level calculations (Figure 2, top).^[44] Additionally, they modified the methylidene unit in these catalysts by substituting hydrogen atoms with fluorine.

Over the subsequent three years, their analysis expanded to include the entire eighth group of the periodic table (Figure 2, bottom).^[45] As expected, ruthenium and osmium demonstrated a clear preference for a singlet ground state. In contrast, iron exhibited multiple accessible spin states, including singlet, triplet, and quintet, all lying energetically close to one another. This near-degeneracy complicates predictions of reactivity and stability,^[46,47] further highlighting the unique electronic properties of iron compared to its heavier congeners. In general, spin-splittings are an exceedingly difficult problem for the whole of computational chemistry.^[48,49] The typical errors associated with DFT approaches can span several dozens of kcal/mol, often requiring costly *ab initio* methods even for the simplest systems. This represents the main source of error in modeling these catalysts, exceeding all other contributing factors.

Conversely, when the metal center is lighter, the bond dissociation energies (BDEs) of both the phosphine ligand in the

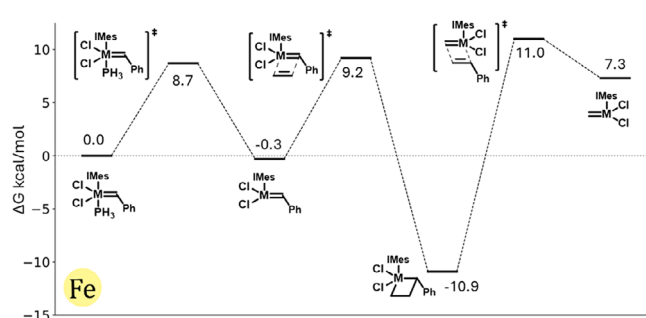


Figure 3. Reaction pathway (Gibbs energies in kcal/mol) computed by Poater and coworkers with ethylene at M06/cc-pVTZ~SDD(PCM, dichloromethane)//BP86/TZVP~SDD level.

precatalyst and the alkene ligand in the 16-electron coordination intermediate decrease (see Figure 2, grey pathways, specifically the transition from the 14e species II to the coordination intermediate III). This reduction poses a challenge, as it impairs the cycloaddition step required for metallacyclobutane formation and instead favors alkylidene transfer.

The introduction of fluorine further decreases the BDE values for all ligands across the coordination intermediates of each metal. However, the trends observed for iron appear to be less predictable and intuitive.^[50] To provide a more in-depth comparison of the thermodynamic and kinetic behaviors of ruthenium and iron, Poater and Cavallo conducted a study using a more structurally detailed model.^[51] Their approach incorporated ligands such as mesityl-substituted *N*-heterocyclic carbene (NHC) ligands,^[52] phosphines, and benzylidenes (see Figure 3). While this model was less computationally accurate including such realistic structural details was essential, as even minor modifications in catalyst design can determine whether a system is catalytically active.

For all calculated iron structures, the singlet state was found to be the ground state, except for the 14-electron species. In these cases, the quintet state was the most stable in Figure 3 with the triplet following closely behind. This reduced singlet stability is consistent with the findings of Dixon's studies.^[44,45] Additionally, the low BDE values associated with olefin coordination suggest that Dixon's model may have overestimated them. Neither the first nor the second coordination intermediate could be obtained, as the olefin was dissociated during geometry optimizations, likely due to steric hindrance from the mesityl groups.^[53,54]

In both cases, reducing the metal-alkene bond distance directly led to metallacyclobutane formation. However, this behavior was expected to change when more electron-rich olefins were used. Indeed, a subsequent study by the same authors confirmed the following premise: when methylvinyl ether was introduced as a ligand, the coordination intermediate could be successfully obtained (see Figure 4).^[55] This second study focused on activation differences between fourth-period and fifth-period transition metals. The activation mechanism of the iron-based catalyst was found to be analogous to that of second-generation Grubbs-type ruthenium catalysts, proceeding via dissociation of the labile ligand. However, the process

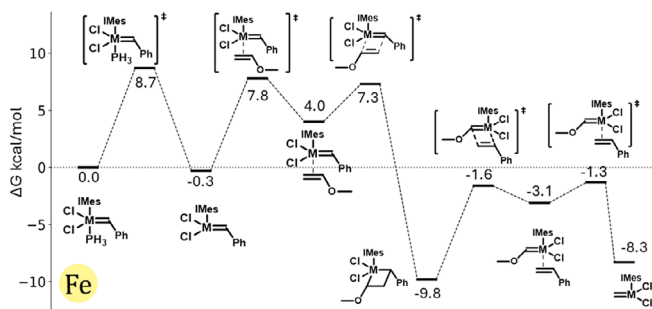


Figure 4. Reaction pathway (Gibbs energies in kcal/mol) computed by Poater and coworkers in 2014 with an alkoxy-based alkene (BP86/Def2TZVP ~SDD(PCM, dichloromethane)).^[55]

required less activation energy when iron was used as the metal center, in agreement with the BDE values previously reported by Dixon.

One drawback of the previously discussed studies is their omission of the cyclopropanation reaction (see Figure 5, top), which may be considered a competing side reaction. Properly assessing the system's chemoselectivity between olefin metathesis and cyclopropanation is crucial, as it directly impacts the catalyst's practical applicability. Addressing this, Solans–Monfort's group incorporated cyclopropanation into their computational models, investigating how ligand modifications influence the

iron catalyst's tendency for carbene transfer.^[56] Their study began with reference calculations on second-generation Grubbs ruthenium catalysts (see Figure 5, left). In these systems, cyclopropanation was determined to be an endergonic process occurring at a considerably slower rate than olefin metathesis. However, when the triplet state was enforced, the preference shifted dramatically toward cyclopropanation. Fortunately, the singlet state remained the ground state, aligning with experimental data and preventing undesired reactivity in ruthenium-based systems. In contrast, when ruthenium was replaced with iron under identical conditions, both spin states exhibited nearly identical energy levels (see Figure 5, right). As a result, cyclopropanation became an almost barrierless process with high exergonicity.

To mitigate this issue, the authors proposed minimal structural modifications to steer the system toward the desired reactivity (see Table 1, top). These adjustments involved replacing conventional chloride ligands with stronger sigma-donors, such as cyanide and alkyl groups. It is well-established that increasing sigma donation to the metal center raises the d-orbital energy splitting, making electron promotion to the triplet state more difficult. Consequently, this substitution elevated the energy of the triplet 14-electron carbene states, though not to the same degree as observed in the ruthenium reference system. Unfortunately, this did not extend to the metallacyclobutane

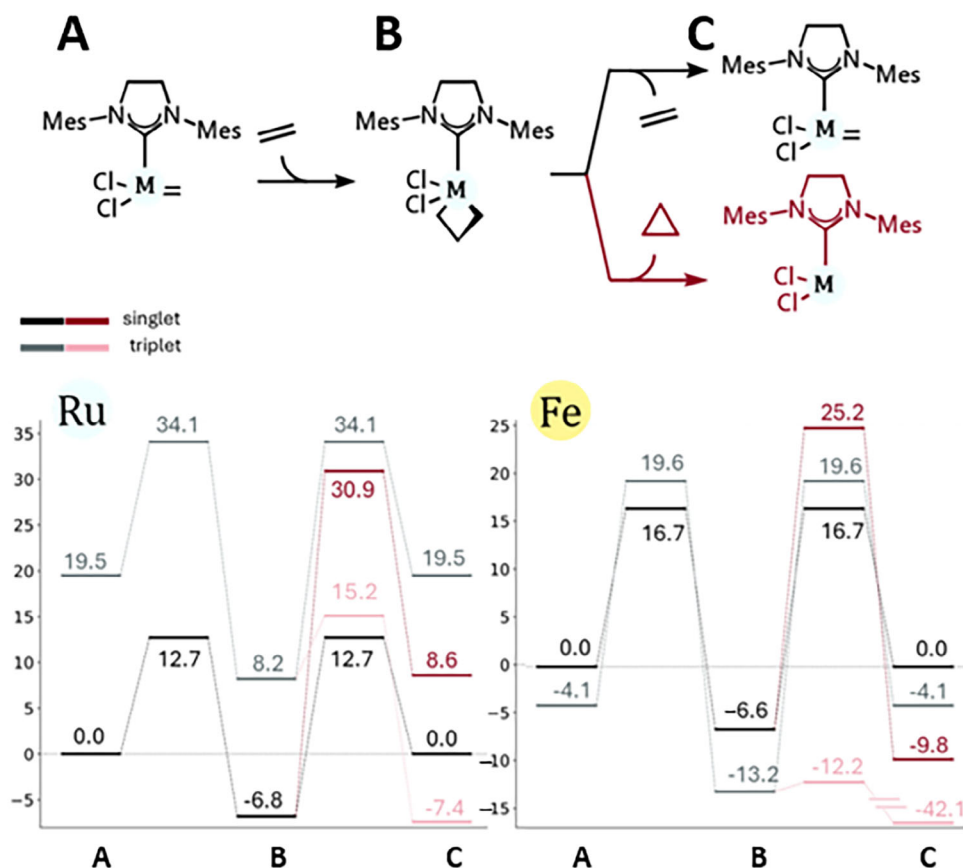


Figure 5. Gas phase Gibbs energy profiles (in kcal/mol) for the metallacyclobutane formation and cyclopropanation (top) for both singlet and triplet multiplicities, for ruthenium (left) and iron (right) at OPBE-D2/6-311++G(d,p)//OPBE-D2/6-31G(d,p) level of theory, including special basis sets for iron and ruthenium, for which pseudopotentials were applied.^[56]

Table 1. Relative Gibbs energies (gas-phase, kcal/mol) of key intermediates (14-electron carbene and metallacyclobutane in Scheme 1). Iron catalysts proposed by Solans–Monfort involving stronger σ -donors (N/A = not available).^[56]

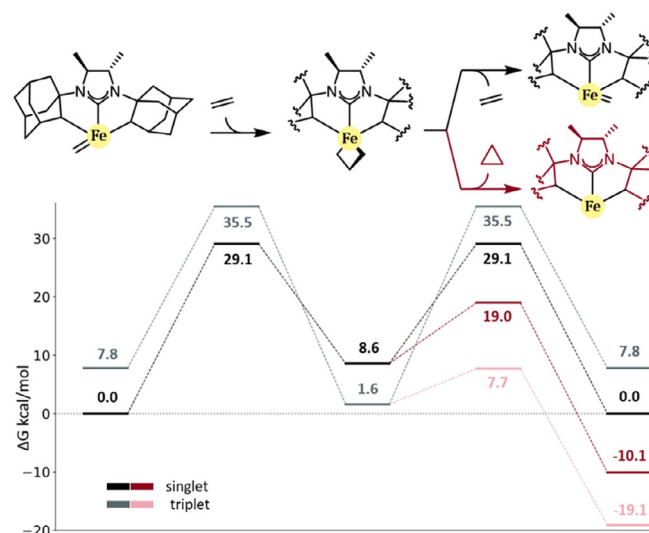
Complex	14-Electron Carbene			Metallacyclobutane		
	Singlet	Triplet	Quintet	Singlet	Triplet	Quintet
	0.0	19.5	49.1	−6.8	8.2	45.7
	0.0	−4.1	−5.2	−6.6	−13.2	−1.4
	0.0	4.5	N/A	−14.9	N/A	N/A
	0.0	4.5	9.9	16.1	6.7	3.6

Table 2. Relative Gibbs energies (gas phase, kcal/mol) of key intermediates (14-electron carbene and metallacyclobutane in Scheme 1). The iron catalysts proposed by Solans–Monfort including C–H activated chelated NHC ligands.^[56]

Complex	Carbene			Metallacyclobutane		
	Singlet	Triplet	Quintet	Singlet	Triplet	Quintet
	0.0	19.5	49.1	−6.8	8.2	47.5
	0.0	4.3	26.9	−13.5	−5.9	3.4
	0.0	3.8	21.0	−11.3	−11.8	0.1
	0.0	6.2	22.7	−18.6	−9.9	−0.6
	0.0	2.7	24.1	−15.2	−10.5	−1.7

intermediate, as shown in Table 1. Ultimately, the study concluded that sigma-donation alone is insufficient to effectively suppress cyclopropanation. However, unfortunately none of the predicted structures have yet been reproduced experimentally.

Solans–Monfort and coworkers then suggested employing Grubbs C–H activated chelate ligands (shown in Table 2,

**Figure 6.** Gibbs energy profile (in kcal/mol) for metallacyclobutane formation and alkene metathesis processes, in both singlet (black) and triplet (gray) states. Cyclopropanation (red, light (singlet), and dark (triplet)).

top).^[56] This proposal was inspired by the work of Veige and coworkers,^[57] who demonstrated that tridentate ligands could enhance the stability of the metallacyclobutane. While these modifications slightly increased its stability, the triplet state still remained the ground state. However, when evaluating the overall thermodynamics of the chelated system, even though the cyclopropanation is still favored with respect to the alkene metathesis, a significant shortening of the kinetic cost was observed for the latter process (Figure 6).

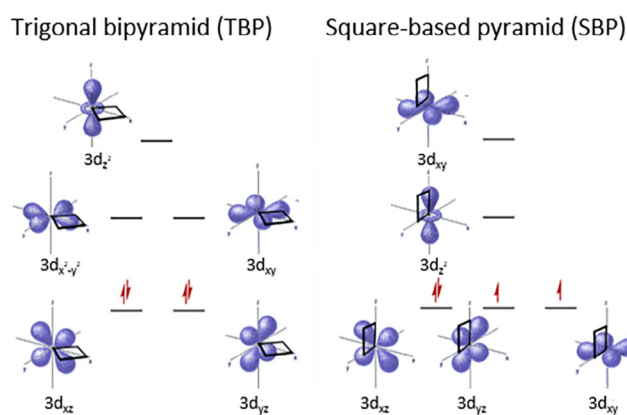


Figure 7. Molecular orbital diagrams of the trigonal bipyramid geometry (left) and square-based pyramidal (right) of the metallacyclobutane complexes of Solans-Monfort.^[56]

Table 3. Relative Gibbs energies (in kcal/mol) from the carbene to the metallacyclobutane complexes of Solans-Monfort, compared to the second-generation Grubbs catalyst.^[56]

Complex	14-Electron Carbene			Metallacyclobutane		
	Singlet	Triplet	Quintet	Singlet	Triplet	Quintet
	0.0	19.5	49.1	-6.8	8.2	45.7
A	0.0	7.2	19.7	-0.7	-7.3	3.1
B	0.0	7.8	19.6	-0.3	-6.0	3.7

3. Metallacyclobutane Intermediate

Solans-Monfort also examined the correlation between spin multiplicity and the geometry of the iron metallacycle coordination complex.^[56] They observed that, in most cases, the trigonal-bipyramidal (TBP) structure in the singlet state shifted to a square-based pyramidal configuration in the triplet state. This transition was explained using the orbital diagram of pentacoordinate complexes and the associated changes in d-orbital degeneracy (Figure 7). Additionally, the authors noted that, unlike the TBP arrangement, square-based pyramidal (SBP) structures position a carbon atom of the olefin *trans* to the central coordinating pincer ligand. Consequently, they proposed that a strongly donating central ligand could destabilize the SBP structure and, therefore, the triplet state of the metallacycle. Based on these findings, several square planar complexes incorporating rigid chelate moieties were suggested for further investigation (Table 3).

Regarding the ground state multiplicity, the newly proposed systems exhibited results similar to those of the C–H activated

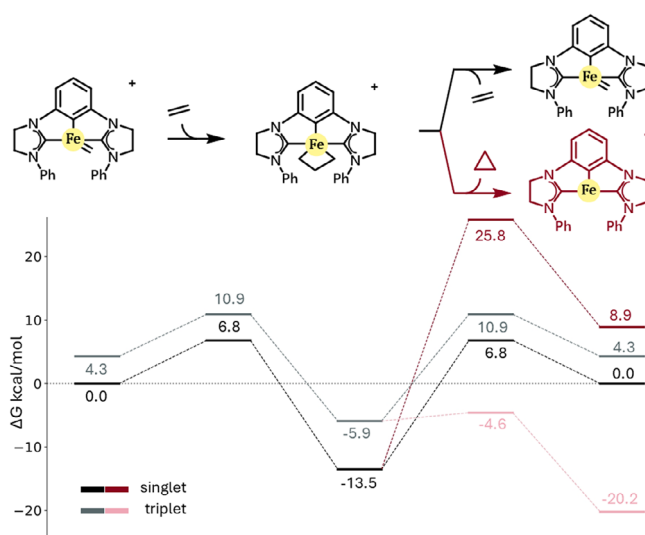


Figure 8. Gas phase Gibbs energy profiles (in kcal/mol) for the metallacyclobutane formation and cyclopropanation (top) for both singlet and triplet multiplicities for a pincer-Fe complex.

chelated systems for the carbene (triplet state ~ 7.0 kcal/mol, compared with data in Table 2), but demonstrated significantly improved performance for the metallacycle, that is, the triplet state of the metallacycle is lower in energy than the singlet. In fact, when considering this aspect, the outcomes even surpassed those of the ruthenium reference system. Furthermore, in these pincer-like ligands, the cyclopropanation reaction became highly endergonic in all singlet state cases (see Figure 8), even though in triplet state the process is barrierless apart from highly exergonic.

In alignment with previous studies^[51,55] stabilizing the singlet state of the carbene is essential for the viability of iron catalysts in olefin metathesis. This can be achieved by introducing stronger sigma-donating ligands. However, the metallacycle still predominantly favors the triplet state, which promotes undesired cyclopropanation. To counteract this, the use of tridentate pincer ligands with a strong σ -donor group in the central position has been proposed. This strategy enforces a trigonal bipyramidal geometry, thereby destabilizing the triplet state. Additionally, the presence of strong donating ligands strengthens the $M=CH_2$ bond, reducing the likelihood of cyclopropanation.

Two years later, in 2018 Solans-Monfort further explored this subject, shifting focus to pentacoordinate systems.^[58] In coordination chemistry, the oxidation state of the metal center plays a crucial role in determining orbital energetics. A higher positive charge on the metal center enhances ligand donation, increasing d-orbital splitting and favoring low-spin configurations such as the singlet state. To leverage these effects for iron-based olefin metathesis catalysis, ligands were chosen to stabilize high-valent iron-oxo complexes, as demonstrated by Costas and coworkers^[59–61] drawing inspiration from experimentally validated cases (Figure 9). In particular, the computational proposal led to stabilize the metallacycle intermediate.^[58]

Many of the previous findings regarding the advantages of sigma-donating ligands and chelating structures in stabilizing

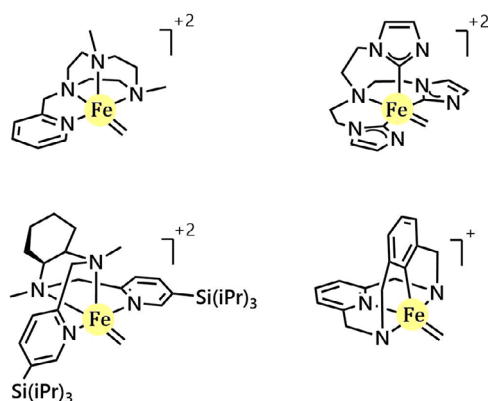


Figure 9. Tetradentate chelate iron-complexes proposed by Solans–Monfort in order to stabilize metallacycle intermediate^[58] with a singlet ground state.

the singlet state were reaffirmed. Notably, the most effective systems were those incorporating chelating ligands with strong sigma donors, while featuring a weaker sigma donor *trans* to the carbene.

Additionally, reducing iron to its formal Fe(0) oxidation state was found to further stabilize the singlet configuration in both key intermediates. In fact, the thermodynamic behavior of certain $L_4Fe(0) = CH_2$ carbene species closely mirrored that of the highly efficient Grubbs second-generation catalyst in metathesis and cyclopropanation reactions. However, a key drawback emerged: for the most promising candidates, the energy barriers for olefin metathesis were still higher than those for cyclopropanation. This issue was primarily linked to the $L_4Fe(0) = CH_2$ complex being in an 18-electron state, which hindered the necessary cycloreversion step. The authors suggested that using labile ligands could resolve this limitation, but they also noted that once ligand dissociation occurs, cyclopropanation would likely become the preferred reaction pathway.^[58]

4. Successful Iron Catalyzed ROMP

Despite extensive computational studies,^[51,55,56,58] only two experimental examples of iron-catalyzed olefin metathesis, in particular ring-opening metathesis polymerization (ROMP), have been identified, with real successful catalytic results. Surprisingly, none aligns with the computational models described previously, both complexes are high-spin and deviate from the suggested geometric patterns.

The first reported case is detailed in a 2021 communication by Bukhryakov and coworkers.^[62] In Figure 10, a well-defined iron catalyst was identified as a bisalkoxide homoleptic complex, capable of performing ring-opening metathesis polymerization of norbornene, producing highly stereoregular polynorbornene with up to 99% *cis* in a syndiotactic way.

Characterization of the synthesized polymers revealed notably high molecular weights and polydispersity indices (PDI), indicative of initiators with activation rates lower than propaga-

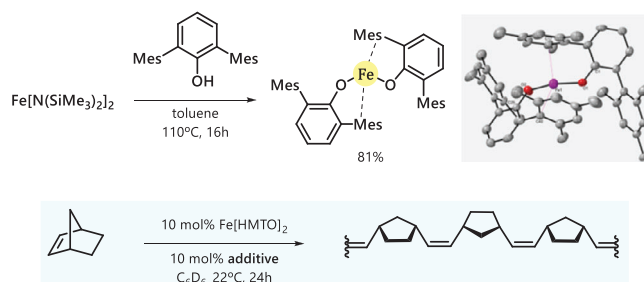


Figure 10. Iron system active on stereospecific ROMP of norbornene (NBE) proposed by Bukhryakov in 2021.^[62]

Table 4. Summary of the conditions tested by Bukhryakov and coworkers (M_n = number-average molecular weight and M_w = weight-average molecular weight).^[62]

Additive	T (°C)	Conv. (%)	<i>Cis/Trans</i>	Tacticity	M_n (g/mol)	M_w/M_n
None	22	16	99:1	Synd.	262800	2.33
$(CF_3)_2CHOH$	22	42	91:9	Synd.	590000	2.22
$Ph(CF_3)_2COH$	22	84	>99:1	Synd	930700	1.97
$Ph(CF_3)_2COH$	70	28	>99:1	Synd	362100	2.30
$Ph(CF_3)_2COH$	100	10	>99:1	Synd	82300	3.31
$Ph(CF_3)_2COH$	−35	43	>99:1	Synd	565700	2.36

tion rates. Additionally, a significant portion of the iron complex in the reaction medium remained unaltered.

Various additives were evaluated, with fluorinated alkoxides such as $(CH_3)_2CF_3CO$, $CH_3(CF_3)_2CO$, or $Ph-(CF_3)_2CO$ enhancing the reaction rate and polydispersity while maintaining tacticity. It was hypothesized that these additives formed corresponding heteroleptic iron alkoxides upon substituting one of the original HMTTO ligands (HMTTO = O-2,6-(2,4,6-Me₃C₆H₂)₂C₆H₃).

Interestingly, fluorinated alcohols with a hydrogen atom on the α -carbon (e.g., $(CF_3)_2CHOH$) led to decreased selectivity (*cis/trans*) and reduced both conversion and molecular weight to half of that observed with $Ph-(CF_3)_2CO$. In fact, $Ph-(CF_3)_2CO$ was identified as the most effective additive at 22 °C. Focusing on this, a decrease in activity was observed as the reaction temperature increased, suggesting decomposition of the active species. Indeed, lowering the temperature yielded better results than heating (see Table 4). Since the M_w/M_n ratios are close to two or over, there is a distribution of chain lengths, with broader molecular weight distribution.

The authors conducted a series of attempts to elucidate the mechanism. In the context of computational studies, both iron ylide and metallacycle can be described as low-spin complexes. However, the authors report that no diamagnetic signal was detected during the reaction, which rules out the involvement of alkylidene-based active species and the metallacycle intrinsic to Chauvin's mechanism.^[63,64] Furthermore, the addition of cyclooctene or octa-1,7-diene during the reaction did not result in their incorporation into the final polymer. This observation is incompatible with the hypothesis of an iron-carbene active species.

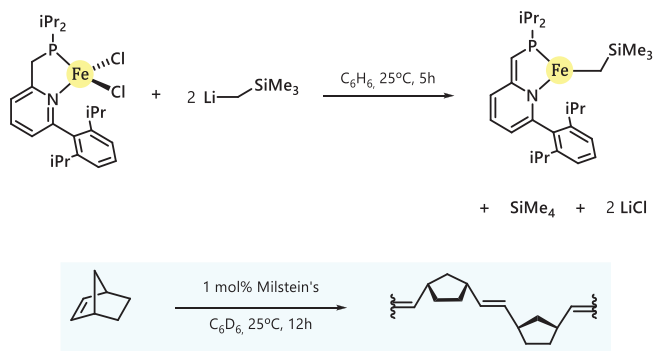


Figure 11. Iron system active on stereospecific ROMP of NBE proposed by Takebayashi, Milstein, and coworkers in 2022.^[65]

Regarding the observed tacticity, the authors cited comparable findings with molybdenum and tungsten, where the chiral nature of Schrock-type catalysts is deemed responsible for the observed ordering. However, this is incompatible with the homoleptic nature of the presented iron system. As a result, the authors proposed that a polynuclear iron aggregate may provide a more accurate explanation, although this still does not explain the apparent lack of iron-carbene.

A redox-initiated ROMP mechanism was also considered, which typically involves a photosensitive additive and the formation of radical intermediates. However, the reaction remained unchanged upon the addition of 3,4-dihydro-2H-pyran or light exposure. Moreover, radical-based ROMPs generally render atactic chains.

Lastly, the possibility of a carbonyl-olefin metathesis (COM) mechanism was explored due to the presence of metal-alkoxide bonds. This was investigated by adding carbonyl compounds to the reaction, but no improvement in ROMP was observed, suggesting that this mechanism is unlikely.

In summary, the study by Bukhryakov and coworkers presents a significant advancement in the field of ROMP using a well-defined iron catalyst. The two-alkoxide homoleptic complex demonstrated exceptional stereoregularity and high molecular weights in the polymerization of norbornene. The investigation into various additives revealed that fluorinated alkoxides, particularly $\text{Ph}(\text{CF}_3)_2\text{CO}$, significantly improved reaction rates and polydispersity while maintaining high tacticity. The study also explored the effects of temperature on the reaction, finding that lower temperatures favored better outcomes. Despite extensive mechanistic studies, the exact nature of the active species remains elusive, with the authors proposing a polynuclear iron aggregate as a potential explanation. Overall, this research provides valuable insights into the optimization of ROMP processes and the role of iron catalysts in achieving high-performance polymers.

More recently, Takebayashi, Milstein, and coworkers have successfully demonstrated the ROMP of a range of cyclic olefins,^[65] including NBE and its derivatives, as well as substituted cyclopropene, by using a tricoordinate iron(II) catalyst. The catalyst features a bidentate ligand, previously pyridine-based, and a (trimethylsilyl)methylene group, which together form a trigonal planar high-spin Fe(II) complex (see Figure 11). A distinctive

feature of this catalyst is the formation of carbenes, which is suggested to occur following the coordination of norbornene. This process involves the elimination of the α -hydrogen from the alkyl ligands and the re-aromatization of the pyridine. It is proposed that this step is rate-determining. The reaction then proceeds via the Chauvin mechanism, forming a metallocyclobutane intermediate, which the authors hypothesize exists in a triplet state. This intermediate undergoes topomerization, involving the internal rotation of the $\text{Fe}=\text{C}$ bond from an apical to an equatorial position, yielding pure *trans*, isotactic polynorbornene with a high molecular weight. Moreover, the polymer formed was identified as only containing E-double bonds, imposing complete *trans*-selectivity, even though it is derived from a *cis*-alkene monomer like NBE. The authors claim this to be unprecedented even among the already known ROMP-catalysts.



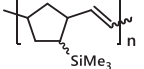
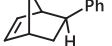
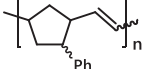


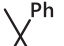
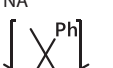
The addition of 0.5 equiv of water notably enhanced the catalyst's activity. However, exceeding one equiv of water led to catalyst deactivation. Introducing an equivalent of water during an ongoing polymerization resulted in the premature cessation of the ROMP before completion. Additional experiments, not detailed here, suggested that water may act as a cocatalyst rather than forming a new catalyst. Unfortunately, the precise role of water could not be elucidated.

The substrate scope was examined, including derivatives of NBE and strained alkenes. Interestingly, functionalities of similar size exhibited different behaviors: silyl and phenyl functionalities (e.g., $-\text{SiMe}_3$ and phenyl) yielded substituted homologous polymers, while oxygen-containing substituents resulted in complete inactivity (see Table 5). The authors attribute this to the potential coordination ability of the latter cases, noting that another inactive complex was observed with the addition of (dimethylamino)pyridine, which also introduces an additional coordination element in the form of nitrogen. Surprisingly, minor modifications to NBE, such as adding a second double bond distant from the reacting one, also showed no reactivity. Moreover, the catalyst's activity appears to be highly dependent on the monomer's ring strain. Indeed, no ROMP product was observed with other low-strain cycles like cyclooctene and cyclopentene. However, the more strained norbornadiene remains unreactive. When testing other strained candidates, although cyclopropene underwent polymerization, the obtained chain corresponded better to an addition-polymerization mechanism rather than a ROMP reaction.

The authors sought to elucidate the mechanism behind the observed reactivity using a combination of experimental and computational techniques. While some mechanistic conclusions have already been discussed to rationalize the observed selectivity, the authors provide a more detailed justification. This is particularly significant, as Bukhryakov's findings suggest that the formation of the polymer does not necessarily imply the occurrence of the ROMP reaction (i.e., Chauvin's mechanism).^[62]

Regarding the initiation step, although it was previously highlighted that this would be slower than propagation, the exact nature of the initiation was not specified. Arising from the observed addition-based polymerization of cyclopropene

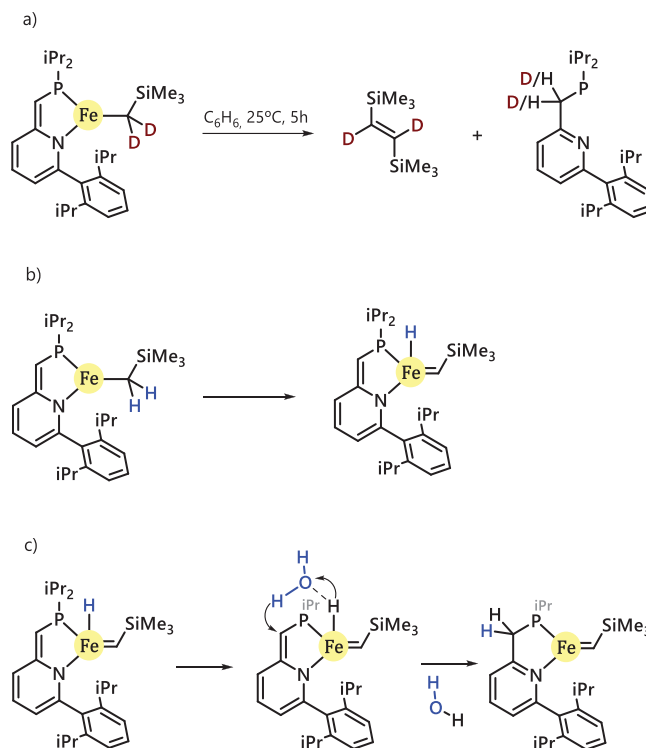
Table 5. Some of the most relevant cyclic olefins tested by Milstein in their system.^[65]

Olefin	Polymer	Time (h)	Isolated Yield (%)
	<i>trans</i> -polyNBE	12	> 99
		16	56
		16	> 99
 R = COOEt, OH, Si(OEt) ₃ , CONH ₂	NA	16	0
	NA	65	0
		7	84

(see last entry in Table 5), the authors initially considered an organic radical mechanism.^[66] However, electron paramagnetic resonance monitoring indicated the absence of unpaired electrons, ruling out a radical mechanism. Notably, upon introducing styrene as a potential chain transfer inducer, while the stereoselectivity and tacticity of the polynorbornene remained unaltered, methylene and phenylmethylene end groups were observed in the polymer. This result demonstrates that the catalyst is capable of promoting cross-metathesis between the polymer chain and styrene, enhancing solubility. However, the absence of stilbene and cyclopropanation products when styrene was reacted with the catalyst in the absence of norbornene indicates that such coupling capability is indeed limited.

The initiation mechanism involving the generation of an iron–carbene complex through α -hydrogen elimination was investigated.^[67] Thermolysis experiments conducted at 90 °C using Milstein's catalyst resulted in the formation of 1,2-bis(trimethylsilyl)ethylene.^[65] Repeating the experiment with the α -carbon deuterated yielded 1,2-bis(trimethylsilyl)ethylene-*d*₂ as the outcome (see Figure 12a). The observation of this product provides evidence supporting the existence of an iron–carbene bond in each of the two coupling parts of the decomposition (see Figure 12b).

Subsequently, attempts were made to trap the corresponding iron–carbene complex. In this system, the carbene is expected to form in situ, though similar formation pathways exist.^[68] Upon testing several alkenes, the authors observed isomerization of 1-octene and 2-octene under ROMP reaction conditions. This suggests the presence of transient iron–hydride species in the reaction, potentially formed via α -hydride elimination. This hypothesis was further supported by adding styrene to the reaction medium and using a deuterated catalyst at the α -carbon position.^[69–71] The reversible proton-transfer process resulted in the formation of deuterated styrene after some reaction time. Additionally, a detailed comparison of the ROMP rate with both the original and α -deuterated catalysts indicated a kinetic isotopic effect ($KIE = 2.36 \pm 0.088$), consistent with the proposed mechanism.

**Figure 12.** Milstein's tests on initiation mechanisms on their system.^[65]

(a) Decomposition products with deuterated atoms in the rearomatized pyridine group. (b) Formation of an iron–carbene via α -hydrogen elimination. (c) Proton transfer-based initiation assisted with water.

From the iron–hydride, a logical next step would be a proton transfer to the pincer ligand, facilitating the re-aromatization of its pyridine moiety. Interestingly, this reaction step is enhanced by water, which explains the increased rates previously observed (see Figure 12c for suggested water-assisted proton transfer).

Despite considerable support for a mechanism involving α -hydride elimination to form an iron hydride and subsequent proton transfer to re-aromatize the pincer ligand, DFT calculations conducted by the authors here yielded energies that were

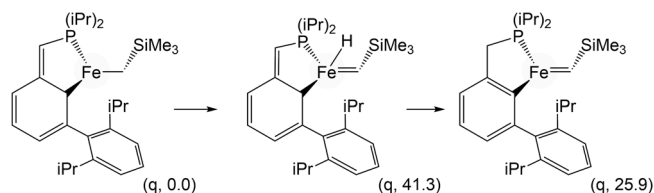


Figure 13. Computed initiation mechanism by Milstein's group^[65] following the DFT model M06L-D4/def2-TZVPPD/SMD(benzene)//M06L-D3/def2-SVP. The multiplicity of each intermediate corresponds to the most stable in each case (relative Gibbs energies in kcal/mol between parentheses).

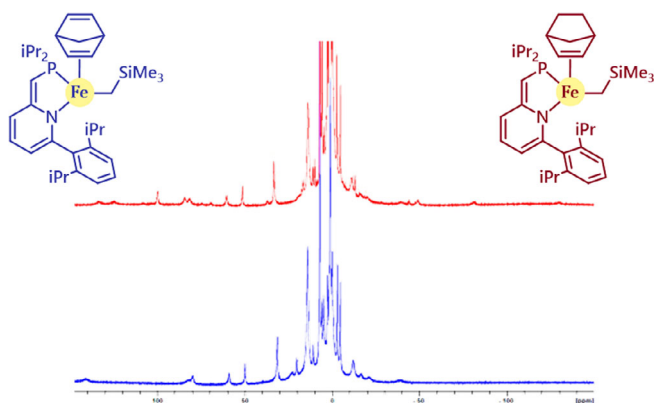


Figure 14. Proton nuclear magnetic resonance proving compelling similarity between the isolated norbornadiene and the non-isolated norbornene complexes.

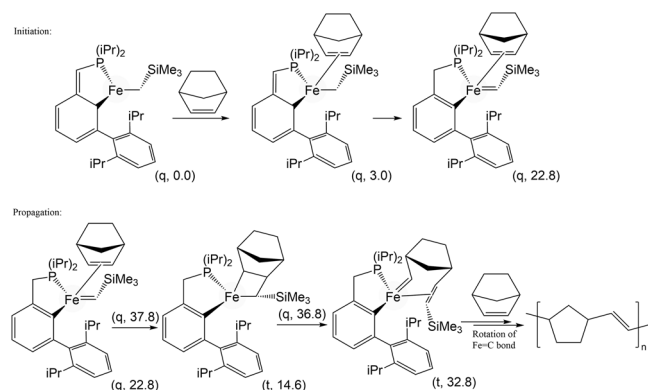


Figure 15. Initiation and propagation mechanisms studied by Takebayashi, Milstein, and coworkers (relative Gibbs energy values in kcal/mol between parentheses).^[65]

too high for the intermediates involved (see Figure 13). In particular, the iron-hydride intermediate exhibited an energy of approximately 41 kcal/mol, making the entire catalyst initiation kinetically unfeasible under the room temperature conditions in which the reaction proceeds.

In this case, it is important to recognize that computational results should not be considered more reliable than experimental data, which, as mentioned earlier, provides strong evidence for the formation of iron hydrides,^[72] bearing in mind that their synthesis is not trivial,^[73–76] with problems in their formation^[21,77–80] and characterization,^[81–84] particularly by DFT calculations.^[85,86] On the other hand, discrepancies between

experiments and calculations may be originated from the accurate designation of spin states of iron-based catalytic systems, which can be challenging for either DFT methods or spectroscopic techniques such as Mössbauer and SQUID magnetometry measurements.^[87–89] What can be inferred from this analysis is that a key aspect of the actual iron hydride may not be considered in either the chemical mechanism or the computational model. Therefore, the possibility of hydride-transfer initiation should not be ruled out.

An alternative initiation pathway was proposed, where coordination of NBE is required. Although the exact reasons for norbornadiene's inactivity remain unclear, Takebayashi, Milstein, and coworkers were able to use it to trap a potential intermediate in the activation process.^[65] The paramagnetic complex formed resulted from a double-bond η^2 coordination of the cyclic hydrocarbon to the Fe center. Following this, while trapping an intermediate with NBE was not successful, monitoring the reaction at low temperatures allowed for the detection of a paramagnetic entity. Its H-NMR pattern closely matches that of an isolable intermediate from norbornadiene (shown in blue in Figure 14).

DFT calculations have been employed to investigate the initiation mechanism of ROMP using iron catalysts (Figure 15). These studies suggest that the energy barriers for the formation of iron-carbene complexes are significantly lower than those proposed via earlier hydride transfer models,^[58,65,90,91] indicating that carbene formation is feasible at ambient temperatures.^[92] In these models, the activated initiator complex is approximately 22.8 kcal/mol higher in energy than the starting complex. The subsequent propagation step involves the formation of intermediates and transition states, with activation barriers that are relatively high for reactions proceeding at room temperature. Notably, the original calculations were based on the NBE-activated complex rather than the precatalyst, which may result in lower apparent activation energies. These findings help explaining why initiation is observed to be slower than propagation in experimental settings. However, due to the inability to obtain transition state data for iron-carbene formation, this explanation remains tentative.

Additionally, Aghazada and coworkers characterized a methyldiene structure using X-ray diffractometry (Table 6).^[93] Specifically, they synthesized, isolated, and analyzed a series of closely related complexes in different oxidation states to validate the electronic structure of the methyldiene complex. Computational analysis supported a Fischer-type electronic description while highlighting strong Fe=CH₂ bond covalency, significant double-bond character, and pronounced alkylidene properties. Computationally, we explored here the feasibility of the methyldiene structure's reactivity with a simple ethylene substrate in olefin metathesis. Surprisingly, the potential formation of the metallacycle was not only kinetically unfavorable but also thermodynamically unfeasible at any multiplicity. Table 6 summarizes the results, showing a reasonable metallacycle but completely incoherent subsequent coordination intermediates, both before and after its formation. Notably, the cleavage of one of the Fe–P bonds with the chelated phosphine is necessary, which explains the presence of two methyldiene species

Table 6. The iron methylidene catalysts proposed by Aghazada, Meyer, and coworkers (with the corresponding X-Ray structure, reproduced with permission from Ref. [93]). Copyright 2021, ACS. Relative Gibbs energies of key intermediates in Scheme 1 (in kcal/mol, method 1: M06L-D3/def2-TZVPP(PCM, dichloromethane)//BP86-D3/def2-SVP; Method 2: M06-D3/def2-TZVPP(PCM, dichloromethane)//BP86-D3/def2-SVP).

Complex	Method 1			Method 2		
	Singlet	Triplet	Quintet	Singlet	Triplet	Quintet
14e Carbene 1	0.0	0.0	0.0	0.0	0.0	0.0
Coordination intermediate 1	33.5	29.2	42.7	33.2	39.8	55.5
Metallacycle	12.8	3.8	11.1	14.9	11.9	24.7
Coordination intermediate 2	47.9	38.3	40.2	47.6	49.0	53.0
14e Carbene 2	31.6	17.0	32.7	33.1	25.4	44.7

Period	Gruppo I. H ⁺	Gruppo II. RO	Gruppo III. R ⁰	Gruppo IV. RR ⁰	Gruppo V. RR ⁰	Gruppo VI. RR ⁰	Gruppo VII. RR ⁰	Gruppo VIII. RO ⁰
1	Li=7	B=5,4	B=11	C=12	N=14	O=16	P=19	
2	Na=23	Mg=24	Al=27,3	Si=28	P=31	S=32	Cl=35,5	
3	K=39	Ca=40	—=44	Ti=48	V=51	Cr=52	Mn=55	Fe=56, Co=59, Ni=59, Cu=63.
4	(Ca=63)	Zn=65	—=68	—=72	As=75	Se=78	Br=80	
5	Rb=86	Sr=87	Yt=88	Zr=90	Nb=94	Mo=96	—=100	Ru=101, Rh=104, Pd=106, Ag=108.
6	(Ag=108)	Cd=112	In=113	Sn=118	Sb=122	Te=125	J=127	
7	Cs=133	Ba=137	?Di=138	?Co=140	—	—	—	
8	(—)	—	—	—	—	—	—	
9	—	—	?Er=178	?La=180	Ta=182	W=184	—	Os=195, Ir=197, Pt=198, Au=199.
10	—	—	—	—	—	—	—	
11	(Au=199)	Hg=200	Tl=204	Pb=207	Bi=208	—	—	
12	—	—	—	Th=231	—	U=240	—	

Figure 16. Mendeleev's 1871 periodic table, where the concept of iso-diagonality was first introduced.

(from M-I to M-II). In fact, this Fe—P bond cleavage accounts for the destabilization of the initial methylidene precatalyst structure. While this may seem like a simple and weak study that led to unfavorable results, it rather confirms that the mechanism initially proposed by Chauvin may not be feasible for any iron-based olefin metathesis catalyst. Instead, the observed experimental activity for other studies in iron olefin metathesis,^[62,65] could be attributed to metal nanoparticles.^[94]

5. The Future of Iron

Despite the advantages previously discussed, iron appears to lack several essential characteristics for effective olefin metathesis. In a recent study, Podewitz and coworkers questioned whether manganese-based catalysts might be more promising than iron-based ones.^[92–95]

They explored the concept of the diagonal or isodiagonal relationship in the periodic table (Figure 16), which refers to the similarities observed between elements that are diagonally adjacent. Notable pairs demonstrating this relationship include lithium and magnesium, or boron and silicon.^[96] These

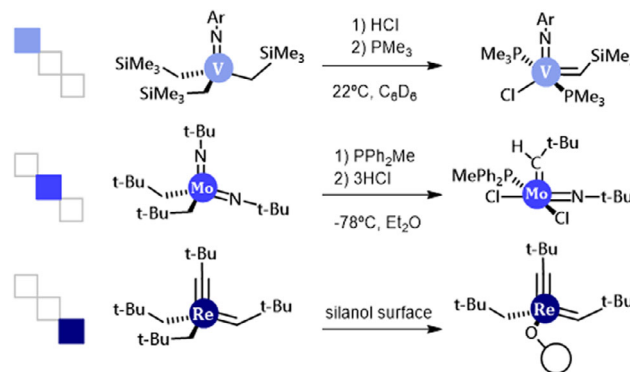


Figure 17. Olefin metathesis active complexes with transition metals showcasing an isodiagonal relationship between them.

pairs exhibit comparable properties, such as similar atomic radii and electronegativities, and analogous compound behaviors. For instance, boron and silicon, both semiconductors, form halides that undergo hydrolysis in water and produce acidic oxides.

While this relationship is traditionally observed among the first 20 elements of the periodic table, recent reports have extended the concept to the d-block elements in organometallic chemistry.^[97] Within the Schrock family of olefin metathesis complexes, a diagonal relationship between molybdenum and vanadium was demonstrated by Bukhryakov and Belov,^[98] who successfully adapted an alpha-hydrogen abstraction reaction from Mo catalyst to a vanadium homologue (Figure 17).^[99,100] Both systems exhibited olefin metathesis activity after phosphine dissociation. Additionally, 14-electron rhenium alkylidene complexes have been reported to be active in olefin metathesis, particularly in achieving highly active silica-supported catalytic systems.^[101,102] Similarly, isodiagonal relationships have been observed between ruthenium (and iridium) with manganese.^[95] Examples include pincer-based complexes for hydrogenation and transfer hydrogenation reactions (Figure 18).

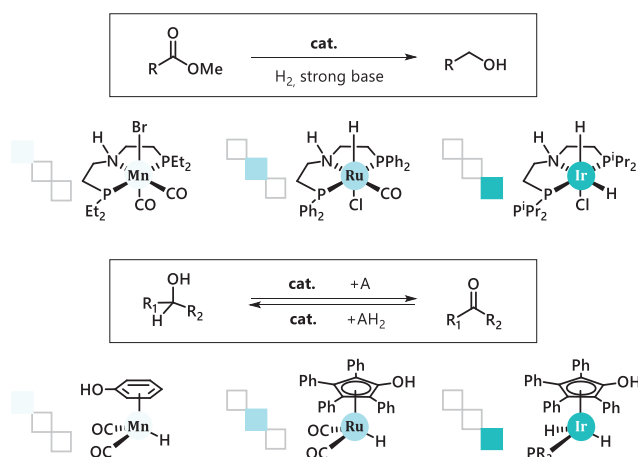


Figure 18. Isodiagonal examples involving manganese, ruthenium and iridium for hydrogenation and hydrogen transfer reactions.^[95]

In their study, Podewitz and coworkers presented a computational work as a preliminary step to guide experimental synthesis toward feasible Mn olefin metathesis catalysts.^[95] They identified challenges with Mn, such as high-spin configurations and weak metal-alkylidene bonds that could lead to undesired cyclopropanation. The study involved a detailed comparison of Fe and Mn complexes with various ligands, assessing the most effective approaches to favor singlet multiplicity.

Notably, the study employed the domain-based local pair natural orbitals coupled-cluster single, double, and perturbative triple (DLPNO-CCSD(T)) method. This approach has demonstrated remarkable accuracy, with results closely aligning with experimental data.^[103–105] The DLPNO variant of the CCSD(T) method is particularly advantageous for assessing singlet and triplet gaps in first-transition series elements, effectively evaluating the multiplicity preference of the system.^[106,107]

6. Manganese Carbenes

Podewitz and coworkers acknowledge the limited number of manganese carbene complexes reported to date.^[95] Among these, most are Fischer-type carbenes, which are prone to rapid cyclopropanation reactions, rendering them unreactive toward olefin metathesis.^[108]

A notable exception is the $\text{MnCp}(\text{CO})_2(=\text{CPh}_2)$ complex reported by Braunschweig and colleagues in 2013.^[109] They explored the isolobal relationship between metal carbenes and borylene-containing metals in group 7, particularly iron borylenes, which exhibit similar reactivity patterns.^[110]

Podewitz et al. in their study (see Figure 19)^[95] examined the nature of the alkylidene bond by using energy decomposition analysis-natural orbital for chemical valence (EDA-NOCV) from the ADF quantum chemistry software, as detailed in Table 7, alongside the Wiberg bond index (WBI). This approach decomposes the total interaction energy (ΔE_{int}) between two fragments into components: electrostatic interaction (ΔE_{elstat}), Pauli repulsion (ΔE_{Pauli}), and orbital interaction (ΔE_{orb}). This decomposition enhances the chemical understanding of the metal-carbene bond, helping determine whether a dative (Fischer-

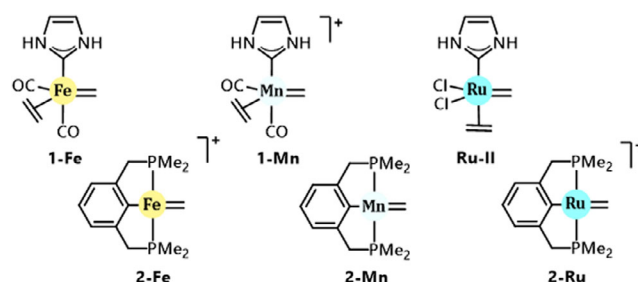


Figure 19. Iron, manganese, and ruthenium systems under comparison by Podewitz and coworkers (following their same labelling for the sake of consistency).^[95]

	Bonding Model	ΔE_{int}	ΔE_{elstat}	ΔE_{orb}	ΔE_{Pauli}
1-Fe	Dative	−114.9	−176.8	−141.2	205.5
	e-sharing	−92.9	−124.0	−139.4	172.9
1-Mn	Dative	−110.7	−198.5	−146.7	238.4
	e-sharing	−95.8	−113.7	−149.4	171.2
Ru-II	Dative	−130.1	−380.8	−322.4	578.8
	e-sharing	−98.7	−158.4	−172.6	237.9
2-Fe	Dative	−126.1	−242.2	−171.4	292.9
	e-sharing	−78.4	−117.1	−155.1	201.2
2-Mn	Dative	−127.6	−220.7	−173.3	271.5
	e-sharing	−86.4	−122.7	−157.9	199.2
2-Ru	dative	−147.0	−306.2	−215.7	379.9
	e-sharing	−106.7	−147.0	−182.3	227.8

type) or electron-sharing (Schrock-type) interaction is more suitable for the system. By imposing closed-shell configurations or triplet states on the fragments, corresponding to the Fischer and Schrock carbene situations respectively, one can evaluate which configuration results in a more favorable ΔE_{orb} .

Ruthenium complexes typically exhibit a lower orbital contribution in their electron-sharing form, favoring the Schrock-carbene configuration instead of the Fischer one, however the reality is that both coexist.^[27] Table 7 shows a lower ΔE_{orb} for the dative (Fischer) interaction. In fact, for all complexes, ΔE_{int} , ΔE_{elstat} , and ΔE_{orb} are more favorable for the dative interaction. However, in all cases, ΔE_{Pauli} is higher for the dative complexes. This suggests that Pauli repulsion may be the dominant factor, at least for the ruthenium center with oxidation state II, which actually exhibits Schrock-type characteristics.^[27] In contrast, manganese and iron systems show a significant different behavior compared to ruthenium. Structurally, the WBI values are 1.70 for 1-Fe and 1.91 for 1-Mn, compared to 2.11 for 2-Fe and 2.19 for 2-Mn, indicating a more pronounced double bond character in the latter systems.

Regarding energy profiles^[95] the 1-Mn system's coordination intermediate in the singlet geometry resembles that of the corresponding iron complex in the triplet state more than in the singlet state. This similarity includes a distorted bipyramidal geometry and a methyldiene dihedral angle not properly aligned for cycloaddition (noncolinear). Additionally, the computed metal-to-alpha carbon distance is 0.1 Å shorter in Mn

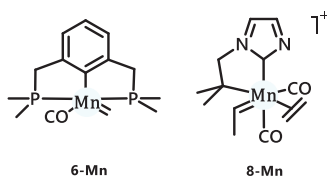


Figure 20. Alternative manganese systems by Podewitz.^[95]

compared to **Fe-1**. Despite the intermediate metallacyclobutane being unexpectedly unstable, olefin metathesis is feasible and kinetically preferred over cyclopropane formation in the singlet state.

Conversely, for the **2-Mn** system, although the triplet state is energetically favored over the singlet in all reaction components, olefin metathesis remains both kinetically and thermally preferred over cyclopropanation decomposition. Furthermore, the cycloaddition becomes an endergonic process in this system.

In cases where one multiplicity state facilitates catalyst deactivation, such as the triplet state in many iron and manganese systems, it is crucial to assess transitions between multiplicity states. The authors calculated the minimal energy crossing points (MECP) for each metallacycle intermediate. For both Mn systems under discussion, the respective MECPs were found to be less than 2.8 kcal/mol from the singlet-metallacyclobutanes, representing thermally accessible surface crossing points. Even in the second system (**2-Mn**), which is selective toward olefin metathesis even in the triplet state, these spin crossings typically lead to undesired reactivity.

Finally, the authors proposed systems that might be more accessible from a synthetic perspective.^[95] Since typical Mn precursors are carbonyl-based, the proposed systems incorporated tridentate ligands with additional CO. Moreover, most known low-spin Mn complexes contain a carbon monoxide moiety, which is advantageous due to its strong donor capabilities. Indeed, for the **6-Mn** system (Figure 20), that is, **2-Mn** including an additional carbonyl on the metal center, the coordination intermediate showed significant stabilization of the singlet state, in detail by 8.1 kcal/mol. However, this candidate and others with a tridentate ligand and CO produced a very strained structure, complicating the octahedral geometry of the metallacyclobutane intermediate. This rigidity ultimately destabilized the singlet state at this key step.

A bidentate alternative was therefore proposed in the form of **8-Mn** (Figure 20). The presence of two CO moieties made the octahedral geometry easily accessible and increased the stability of the metallacyclobutane singlet. Unfortunately, a migratory CO insertion into the carbene was found due to the CO in *trans* to the NHC moiety, leading to a new deactivation pathway.

7. Conclusion

The investigation of iron catalysts for olefin metathesis has provided valuable insights into their potential and limitations. While iron catalysts can be effective, their complex electronic behavior and the challenges associated with stabilizing the desired spin states make their application somewhat constrained. Traditional DFT approaches have shown limitations, particularly

in accurately determining the multiplicity of the ground state configuration.

The geometry and stability of key intermediates, such as the metallacyclobutane, are significantly influenced by the spin state of the iron center. Efforts to stabilize the singlet state through the introduction of strong sigma-donating ligands have shown promise, but issues like undesired cyclopropanation remain a challenge.

Mechanistic studies have highlighted the complexity of iron-catalyzed ROMP, with various potential pathways and intermediates being proposed. Despite extensive research, the exact nature of the active species in these reactions remains elusive, and further experimental and computational studies are needed to fully elucidate these mechanisms. In this context, the formulation of new catalytic models should consider deviations from the well-established Chauvin's mechanism.

The comparative analysis of iron and manganese systems suggests that manganese may offer a promising alternative to iron for olefin metathesis. The recent work by Podewitz and coworkers^[95] which explores the potential of manganese-based catalysts, opens new opportunities for developing more efficient and selective catalysts. The potential relationship between elements in the periodic table, such as iron and manganese, provides a theoretical basis for this approach.

In conclusion, while iron catalysts have shown potential for olefin metathesis, their application is currently limited by several factors. Future research should focus on optimizing ligand environments, exploring alternative metal centers like manganese, and further investigating the mechanistic pathways to overcome these limitations, as well as the concentration effects by microkinetic simulations.^[111] The insights gained from this study provide a foundation for the development of more effective catalysts and open new avenues for research in this field. However, we must be cautious with the existing results on olefin metathesis using iron as the catalyst metal, as the available experimental data are scarce—limited mainly to the work of Bukhryakov, Takebayashi, and Milstein—and completely lacking for manganese. What is more concerning is that even for iron, there has been no follow-up work, which makes these studies difficult to reproduce and poor indicators of a promising future. While DFT calculations do not provide definitive proof, if we are being honest, they might simply validate that the use of iron—especially in olefin metathesis—is far from efficient. Even then, selectivity would still need to be addressed. This should spark a debate: when we reach such a point, should we continue investing further effort? Perhaps the combination of existing results, both theoretical and experimental, should help conclude the topic—at least in this direction.

8. Experimental Details

We employed the Gaussian16 software^[112] to perform static calculations grounded in DFT. For geometry optimizations, we utilized the BP86 functional of Becke and Perdew,^[113–115] incorporating Grimme's D3 dispersion corrections,^[116,117] and described the electronic configurations with the def2-SVP basis set.^[118]

These optimizations were conducted without coordinates constraints, and stationary points were validated through analytical frequency calculations, which also provided zero-point energy (ZPE) and thermochemical corrections. Subsequently, single-point energy calculations were executed using the M06-D3 functional^[119,120] combined with the def2-TZVPP basis set. Solvent effects were modeled using the polarization continuum model (PCM)^[121,122] or the SMD model,^[123] to simulate the influence of dichloromethane. The reported Gibbs energies encompass electronic energies computed at the M06-D3/def2-TZVPP//BP86-D3/def2-SVP level of theory, adjusted for ZPE, thermal corrections, and entropy effects derived from the BP86-D3/def2-SVP calculations (Supporting Information).

Supporting Information

All xyz coordinates and absolute energies (in a.u.) of the not published calculations are available in the supplementary material of this article.

Acknowledgements

Albert Poater is a Serra Hünter Fellow. Albert Poater thanks the Spanish Ministerio de Ciencia e Innovación for project PID2021-127423NB-I00 and the Generalitat de Catalunya for project 2021SGR623. Juan Pablo Martínez acknowledges financial support from the Polish National Science Center through the SONATA-19 grant UMO-2023/51/D/ST4/01561. Jean Luc Renaud gratefully acknowledges financial support from the “Ministère de la Recherche et des Nouvelles Technologies”, Normandie Université, University of Caen Normandie, CNRS, “Région Normandie”, the LABEX SynOrg (ANR-11-LABEX-0029), and European Union (HORIZON-MSCA-2022-DN-01 Project:101119574). The authors thank the reviewers for improving the quality of the paper.

Conflict of Interests

The authors declare no conflict of interest.

Data Availability Statement

The data that support the findings of this study are available in the supplementary material of this article.

Keywords: Cyclopropanation • Iron • Manganese • Metallacycle • Olefin metathesis

- [1] T. K. Olszewski, M. Bieniek, K. Skowerski, *Org. Process Res. Dev.* **2020**, *24*, 125–145.
- [2] G. Szczepaniak, A. Ruszczyńska, K. Kosiński, E. Bulska, K. Grela, *Green Chem.* **2018**, *20*, 1280–1289.
- [3] R. H. Grubbs, P. L. Burk, D. D. Carr, *J. Am. Chem. Soc.* **1975**, *97*, 3265–3267.
- [4] R. H. Grubbs, D. D. Carr, C. Hoppin, P. L. Burk, *J. Am. Chem. Soc.* **1976**, *98*, 3478–3483.
- [5] G. C. Vougioukalakis, R. H. Grubbs, *Chem. -Eur. J.* **2008**, *14*, 7545–7556.
- [6] J. Huang, E. D. Stevens, S. P. Nolan, J. L. Peterson, *J. Am. Chem. Soc.* **1999**, *121*, 2674–2678.
- [7] J. P. Martínez, B. Trzaskowski, *ChemPhysChem* **2022**, *23*, e202200580.
- [8] R. R. Schrock, J. S. Murdzek, G. C. Bazan, J. Robbins, M. DiMare, M. O'Regan, *J. Am. Chem. Soc.* **1990**, *112*, 3875–3886.
- [9] W. C. P. Tsang, J. A. Jernelius, G. A. Cortez, G. S. Weatherhead, R. R. Schrock, A. H. Hoveyda, *J. Am. Chem. Soc.* **2003**, *125*, 2591–2596.
- [10] R. R. Schrock, *J. Am. Chem. Soc.* **1974**, *96*, 6796–6797.
- [11] V. Dragutan, I. Dragutan, L. Delaude, A. Demonceau, *Coord. Chem. Rev.* **2007**, *251*, 765–794.
- [12] O. Eivgi, R. S. Phatake, N. B. Nechmad, N. G. Lemcoff, *Acc. Chem. Res.* **2020**, *53*, 2456–2471.
- [13] *Iron Catalysis in Organic Chemistry* (Ed: B. Plietker), Wiley-VCH, Weinheim, Germany **2008**.
- [14] C. Bolm, J. Legros, J. Le Pailh, L. Zani, *Chem. Rev.* **2004**, *104*, 6217–6254.
- [15] S. Rana, J. Prasad Biswas, S. Paul, A. Paik, D. Maiti, *Chem. Soc. Rev.* **2021**, *50*, 243–472.
- [16] R. Kumar, T. Tewari, S. H. Chikkali, *ChemCatChem* **2024**, *16*, e202400756.
- [17] I. Bauer, H.-J. Knölker, *Chem. Rev.* **2015**, *115*, 3170–3387.
- [18] N. Joly, S. Gaillard, A. Poater, J.-L. Renaud, *Org. Chem. Front.* **2024**, *11*, 7278–7317.
- [19] N. Joly, C. Mauclair, S. Gaillard, A. Poater, J.-L. Renaud, *Asian J. Org. Chem.* **2025**, e202400728.
- [20] P. Rajeshwaran, J. Trouvé, K. Youssef, R. Gramage-Doria, *Angew. Chem. Int. Ed. Engl.* **2022**, *61*, e202211016.
- [21] J. Trouvé, K. Youssef, S. Kasemthaveechok, R. Gramage-Doria, *ACS Catal.* **2023**, *13*, 4421–4432.
- [22] M. Costas, *Coord. Chem. Rev.* **2011**, *255*, 2912–2932.
- [23] L. M. Azofra, S. V. C. Vummaleti, Z. Zhang, A. Poater, L. Cavallo, *Organometallics* **2020**, *39*, 3972–3982.
- [24] A. Poater, F. Ragone, A. Correa, L. Cavallo, *Dalton Trans.* **2011**, *40*, 11066–11069.
- [25] P. De Fremont, N. Marion, S. P. Nolan, *Coord. Chem. Rev.* **2009**, *253*, 862–892.
- [26] P. J.-L. Hérisson, Y. Chauvin, *Makromol. Chem.* **1971**, *141*, 161–176.
- [27] M. Gimferrer, P. Salvador, A. Poater, *Organometallics* **2019**, *38*, 4585–4592.
- [28] M. Mauksch, S. B. Tsogoeva, *Chem. -Eur. J.* **2017**, *23*, 10264–10269.
- [29] E. de Brito Sá, A. Rimola, L. Rodríguez-Santiago, M. Sodupe, X. Solans-Monfort, *J. Phys. Chem. A* **2018**, *122*, 1702–1712.
- [30] *Olefin Metathesis: Theory and Practice* (Ed: K. Grela), Wiley, Hoboken, New Jersey **2014**.
- [31] A. A. Tsedal, *J. Chem.* **2021**, *2021*, 1–14.
- [32] M. Schuster, S. Blechert, *Angew. Chem. Int. Ed. Engl.* **1997**, *36*, 2036–2056.
- [33] M. Rouen, P. Queval, E. Borré, L. Falivene, A. Poater, M. Berthod, F. Hugues, L. Cavallo, O. Baslé, H. Olivier-Bourbigou, M. Mauduit, *ACS Catal.* **2016**, *6*, 7970–7976.
- [34] S. Manzini, A. Poater, D. J. Nelson, L. Cavallo, A. M. Z. Slawin, S. P. Nolan, *Angew. Chem., Int. Ed.* **2014**, *53*, 8995–8999.
- [35] S. Manzini, D. J. Nelson, T. Lebl, A. Poater, L. Cavallo, A. M. Z. Slawin, S. P. Nolan, *Chem. Commun.* **2014**, *50*, 2205–2207.
- [36] S. Manzini, C. A. Urbina-Blanco, A. Poater, A. M. Z. Slawin, L. Cavallo, S. P. Nolan, *Angew. Chem. Int. Ed. Engl.* **2012**, *51*, 1042–1045.
- [37] A. Bailey, M. Foscato, C. S. Higman, C. S. Day, V. R. Vidar, D. E. Fogg, *J. Am. Chem. Soc.* **2018**, *140*, 6931–6944.
- [38] D. L. Nascimento, M. Foscato, G. Occhipinti, V. R. Jensen, D. E. Fogg, *J. Am. Chem. Soc.* **2021**, *143*, 11072–11079.
- [39] J. C. Conrad, D. E. Fogg, *Curr. Org. Chem.* **2006**, *10*, 185–202.
- [40] D. Amoroso, G. P. A. Yap, D. E. Fogg, *Organometallics* **2002**, *21*, 3335–3343.
- [41] A. Poater, N. Bahri-Lalehah, L. Cavallo, *Chem. Commun.* **2011**, *47*, 6674–6676.
- [42] G. Pareras, D. Detiana, A. Poater, *Catalysts* **2020**, *10*, 687.
- [43] B. W. Grau, A. Neuhauser, S. Aghazada, K. Meyer, S. B. Tsogoeva, *Chem. -Eur. J.* **2022**, *28*, e202201414.
- [44] M. Vasiliiu, S. Li, A. J. Arduengo, D. A. Dixon, *J. Phys. Chem. C* **2011**, *115*, 12106–12120.
- [45] M. Vasiliiu, A. J. Arduengo, D. A. Dixon, *J. Phys. Chem. C* **2014**, *118*, 13563–13577.
- [46] K. P. Kepp, *Inorg. Chem.* **2016**, *55*, 2717–2727.

- [47] M. Feldt, Q. M. Phung, K. Pierloot, R. A. Mata, J. N. Harvey, *J. Chem. Theory Comput.* **2019**, *15*, 922–937.
- [48] B. M. Flöser, Y. Guo, C. Riplinger, F. Tuczek, F. Neese, *J. Chem. Theory Comput.* **2020**, *16*, 2224–2235.
- [49] J. Cirera, M. Via-Nadal, E. Ruiz, *Inorg. Chem.* **2018**, *57*, 14097–14105.
- [50] R. Monreal-Corona, A. Pla-Quintana, A. Poater, *Trends Chem.* **2023**, *5*, 935–946.
- [51] A. Poater, S. V. C. Chaitanya Vummaleti, E. Pump, L. Cavallo, *Dalton Trans.* **2014**, *43*, 11216–11220.
- [52] S. Díez-Gonzalez, N. Marion, S. P. Nolan, *Chem. Rev.* **2009**, *109*, 3612–3676.
- [53] S. Escayola, N. Bahri-Laleh, A. Poater, *Chem. Soc. Rev.* **2024**, *53*, 853–882.
- [54] A. Poater, L. Falivene, C. A. Urbina-Blanco, S. Manzini, S. P. Nolan, L. Cavallo, *Dalton Trans.* **2013**, *42*, 7433–7439.
- [55] A. Poater, E. Pump, S. V. C. Vummaleti, L. Cavallo, *Chem. Phys. Lett.* **2014**, *610–611*, 29–32.
- [56] É. De Brito Sá, L. Rodríguez-Santiago, M. Sodupe, X. Solans-Monfort, *Organometallics* **2016**, *35*, 3914–3923.
- [57] M. E. O'Reilly, I. Ghiviriga, K. A. Abboud, A. S. Veige, *Dalton Trans.* **2013**, *42*, 3326–3336.
- [58] É. De Brito Sá, L. Rodríguez-Santiago, M. Sodupe, X. Solans-Monfort, *Organometallics* **2018**, *37*, 1229–1241.
- [59] A. Company, L. Gómez, M. Güell, X. Ribas, J. M. Luis, L. Que Jr., M. Costas, *J. Am. Chem. Soc.* **2007**, *129*, 15766–15767.
- [60] D. Font, M. Canta, M. Milan, O. Cussó, X. Ribas, R. J. M. Klein Gebbink, M. Costas, *Angew. Chem., Int. Ed.* **2016**, *55*, 5776–5779.
- [61] G. Olivo, O. Cussó, M. Costas, *Chem. Asian J.* **2016**, *11*, 3148–3158.
- [62] D. S. Belov, L. Mathivathanan, M. J. Beazley, W. B. Martin, K. V. Bukhryakov, *Angew. Chem. Int. Ed. Engl.* **2021**, *60*, 2934–2938.
- [63] A. Poater, L. Cavallo, *Beilstein J. Org. Chem.* **2015**, *11*, 1767–1780.
- [64] R. Credendino, A. Poater, F. Ragone, L. Cavallo, *Catal. Sci. Technol.* **2011**, *1*, 1287–1297.
- [65] S. Takebayashi, M. A. Iron, M. Feller, O. Rivada-Wheelaghan, G. Leituss, Y. Diskin-Posner, L. J. W. Shimon, L. Avram, R. Carmieli, S. G. Wolf, I. Cohen-Ofri, R. A. Sanguramath, R. Shenhar, M. Eisen, D. Milstein, *Nat. Catal.* **2022**, *5*, 494–502.
- [66] K. A. Ogawa, A. E. Goetz, A. J. Boydston, *J. Am. Chem. Soc.* **2015**, *137*, 1400–1403.
- [67] J. F. Hartwig, *Organotransition Metal Chemistry: From Bonding to Catalysis*, University Science Books, Sausalito, CA **2010**.
- [68] G. C. Vougioukalakis, R. H. Grubbs, *Chem. Rev.* **2010**, *110*, 1746–1787.
- [69] R. M. Bullock, E. G. Samsel, *J. Am. Chem. Soc.* **1987**, *109*, 6542–6544.
- [70] R. M. Bullock, E. G. Samsel, *J. Am. Chem. Soc.* **1990**, *112*, 6886–6898.
- [71] K. R. Delgado, D. D. Youmans, S. T. Diver, *Org. Lett.* **2020**, *22*, 750–754.
- [72] N. Gorgas, B. Stöger, L. F. Veiros, E. Pittenauer, G. Allmaier, K. Kirchner, *Organometallics* **2014**, *33*, 6905–6914.
- [73] G. A. N. Felton, A. K. Vannucci, N. Okumura, L. T. Lockett, D. H. Evans, R. S. Glass, D. L. Lichtenberger, *Organometallics* **2008**, *27*, 4671–4679.
- [74] T. Liu, S. Chen, M. J. O'Hagan, M. R. DuBois, R. M. Bullock, D. L. DuBois, *J. Am. Chem. Soc.* **2012**, *134*, 6257–6272.
- [75] T. Liu, D. L. DuBois, R. M. Bullock, *Nat. Chem.* **2013**, *5*, 228–233.
- [76] T. Liu, X. Wang, C. Hoffmann, D. L. DuBois, R. M. Bullock, *Angew. Chem. Int. Ed. Engl.* **2014**, *53*, 5300–5304.
- [77] R. H. Morris, *Chem. Rev.* **2016**, *116*, 8588–8654.
- [78] S. J. Connelly Robinson, D. M. Heinekey, *Chem. Commun.* **2017**, *53*, 669–676.
- [79] S. Jiang, S. Quintero-Duque, T. Roisnel, V. Dorcet, M. Grellier, S. Sabo-Etienne, C. Darcel, J.-B. Sortais, *Dalton Trans.* **2016**, *45*, 11101–11108.
- [80] S. Kaur-Ghumaan, L. Schwartz, R. Lomoth, M. Stein, S. Ott, *Angew. Chem. Int. Ed. Engl.* **2010**, *49*, 8033–8036.
- [81] M. Malischewski, K. Seppelt, J. Sutter, F. W. Heinemann, B. Dittich, K. Meyer, *Angew. Chem. Int. Ed. Engl.* **2017**, *56*, 13372–13376.
- [82] H.-J. Knölker, E. Baum, H. Goesmann, R. Klaus, *Angew. Chem. Int. Ed. Engl.* **1999**, *38*, 2064–2066.
- [83] D. W. Mulder, Y. Guo, M. W. Ratzloff, P. W. King, *J. Am. Chem. Soc.* **2017**, *139*, 83–86.
- [84] R. J. Kazlauskas, M. S. Wrighton, *Organometallics* **1982**, *1*, 602–611.
- [85] P. A. Dub, J. C. Gordon, *ACS Catal.* **2017**, *7*, 6635–6655.
- [86] F. Bertini, N. Gorgas, B. Stöger, M. Peruzzini, L. F. Veiros, K. Kirchner, L. Gonsalvi, *ACS Catal.* **2016**, *6*, 2889–2893.
- [87] N. U. Din Reshi, D. Bockfeld, D. Baabe, L. Denker, J. P. Martínez, B. Trzaskowski, R. Frank, M. Tamm, *ACS Catal.* **2024**, *14*, 1759–1772.
- [88] M. Pápai, G. Vankó, *J. Chem. Theory Comput.* **2013**, *9*, 5004–5020.
- [89] L. Rousseau, E. Brémond, G. Lefèvre, *New J. Chem.* **2018**, *42*, 7612–7616.
- [90] B. Yang, D. G. Truhlar, *Organometallics* **2018**, *37*, 3917–3927.
- [91] B. P. Jacobs, R. G. Agarwal, P. T. Wolczanski, T. R. Cundari, S. N. MacMillan, *Polyhedron* **2016**, *116*, 47–56.
- [92] Z. S. Lincoln, V. M. Iluc, *J. Am. Chem. Soc.* **2024**, *146*, 17595–17599.
- [93] S. Aghazada, D. Munz, F. W. Heinemann, A. Scheurer, K. Meyer, *J. Am. Chem. Soc.* **2021**, *143*, 17219–17225.
- [94] S. Naeem, S. A. Serapian, A. Toscani, A. J. P. White, J. P. Andrew, G. Hogarth, J. D. E. T. Wilton-Ely, *Inorg. Chem.* **2014**, *53*, 2404–2416.
- [95] J. Pecak, R. A. Talmazan, D. Svatunek, K. Kirchner, M. Podewitz, *Organometallics* **2024**, *43*, 457–466.
- [96] G. Rayner-Canham, *Found. Chem.* **2011**, *13*, 121–129.
- [97] K. Mashima, *Organometallics* **2021**, *40*, 3497–3505.
- [98] K. V. Bukhryakov, S. VenkatRamani, C. Tsay, A. Hoveyda, R. R. Schrock, *Organometallics* **2017**, *36*, 4208–4214.
- [99] G. Tejada, D. S. Belov, D. A. Fenoll, K. L. Rue, C. Tsay, X. Solans-Monfort, K. V. Bukhryakov, *Organometallics* **2022**, *41*, 361–365.
- [100] K. Nomura, S. Zhang, *Chem. Rev.* **2011**, *111*, 2342–2362.
- [101] M. Chabanas, A. Baudouin, C. Copéret, J.-M. Basset, *J. Am. Chem. Soc.* **2001**, *123*, 2062–2063.
- [102] M. Chabanas, C. Copéret, J.-M. Basset, *Chem. -Eur. J.* **2003**, *9*, 971–975.
- [103] G. Bistoni, A. Altun, Z. Wang, F. Neese, *Acc. Chem. Res.* **2024**, *57*, 5039–5048.
- [104] M. Torrent-Sucarrat, S. Navarro, F. P. Cossío, J. M. Anglada, J. M. Luis, *J. Comput. Chem.* **2017**, *38*, 2819–2828.
- [105] N. Villegas-Escobar, A. Poater, M. Solà, H. F. Schaefer III, A. Toro-Labbé, *Phys. Chem. Chem. Phys.* **2019**, *21*, 5039–5048.
- [106] B. Maity, Y. Minenkov, L. Cavallo, *J. Chem. Phys.* **2019**, *151*, 014301.
- [107] M. Drosou, C. A. Mitsopoulou, D. A. Pantazis, *J. Chem. Theory Comput.* **2022**, *18*, 3538–3548.
- [108] T. R. Hoyer, G. M. Rehberg, *Organometallics* **1990**, *9*, 3014–3015.
- [109] J. Bauer, H. Braunschweig, A. Damme, J. O. C. Jimenez-Halla, T. Kramer, K. Radacki, R. Shang, E. Siedler, Q. Ye, *J. Am. Chem. Soc.* **2013**, *135*, 8726–8734.
- [110] A. Matler, M. Arrowsmith, F. Schorr, A. Hermann, A. Hofmann, C. Lenczyk, H. Braunschweig, *Eur. J. Inorg. Chem.* **2021**, *2021*, 4619–4631.
- [111] M. Besora, F. Maseras, W. Interdiscip, *Rev. Comput. Mol. Sci.* **2018**, *8*, e1372.
- [112] M. J. Frisch, G. W. Trucks, H. B. Schlegel, G. E. Scuseria, M. A. Robb, J. R. Cheeseman, G. Scalmani, V. Barone, G. A. Petersson, H. Nakatsuji, X. Li, M. Caricato, A. V. Marenich, J. Bloino, B. G. Janesko, R. Gomperts, B. Mennucci, H. P. Hratchian, J. V. Ortiz, A. F. Izmaylov, J. L. Sonnenberg, D. Williams-Young, F. Ding, F. Lipparini, F. Egidi, J. Goings, B. Peng, A. Petrone, T. Henderson, D. Ranasinghe, *Gaussian 16*, Revision C.01, Gaussian, Inc., Wallingford CT **2019**.
- [113] J. P. Perdew, *Phys. Rev. B* **1986**, *33*, 8822–8824.
- [114] A. D. Becke, *Phys. Rev. A* **1988**, *38*, 3098–3100.
- [115] J. P. Perdew, *Phys. Rev. B* **1986**, *34*, 7406–7406.
- [116] S. Grimme, J. Antony, S. Ehrlich, H. Krieg, *J. Chem. Phys.* **2010**, *132*, 154104.
- [117] S. Grimme, *J. Chem. Phys.* **2006**, *124*, 034108.
- [118] F. Weigend, R. Ahlrichs, *Phys. Chem. Chem. Phys.* **2005**, *7*, 3297–3305.
- [119] Y. Zhao, D. G. Truhlar, *Theor. Chem. Acc.* **2008**, *120*, 215–241.
- [120] Y. Zhao, D. G. Truhlar, *J. Chem. Phys.* **2006**, *125*, 194101.
- [121] V. Barone, M. Cossi, *J. Phys. Chem. A* **1998**, *102*, 1995–2001.
- [122] J. Tomasi, M. Persico, *Chem. Rev.* **1994**, *94*, 2027–2094.
- [123] A. V. Marenich, C. J. Cramer, D. G. Truhlar, *J. Phys. Chem. B* **2009**, *113*, 6378–6396.

Manuscript received: March 29, 2025

Revised manuscript received: May 5, 2025

Accepted manuscript online: May 10, 2025

Version of record online: June 6, 2025